APL Materials

RESEARCH ARTICLE | FEBRUARY 03 2020

Solubility limit and material properties of a κ-$(Al_xGa_{1-x})_2O_3$ thin film with a lateral cation gradient on (00.1)Al_2O_3 by tin-assisted PLD

A. Hassa ; C. Sturm; M. Kneiß ; D. Splith ; H. von Wenckstern ; T. Schultz ; N. Koch ; M. Lorenz ; M. Grundmann

APL Mater. 8, 021103 (2020)
https://doi.org/10.1063/1.5141041

Solubility limit and material properties of a κ-$(Al_xGa_{1-x})_2O_3$ thin film with a lateral cation gradient on (00.1)Al_2O_3 by tin-assisted PLD

Cite as: APL Mater. 8, 021103 (2020); doi: 10.1063/1.5141041
Submitted: 3 December 2019 • Accepted: 14 January 2020 •
Published Online: 3 February 2020

A. Hassa,[1,a] C. Sturm,[1] M. Kneiß,[1] D. Splith,[1] H. von Wenckstern,[1] T. Schultz,[2,3] N. Koch,[2,3] M. Lorenz,[1] and M. Grundmann[1]

AFFILIATIONS

[1]Universität Leipzig, Felix-Bloch-Institut für Festkörperphysik, Linnéstraße 5, 04103 Leipzig, Germany
[2]Humboldt-Universität zu Berlin, Institut für Physik, Newtonstraße 15, 12489 Berlin, Germany
[3]Helmholtz-Zentrum für Energie und Materialien GmbH, Hahn-Meitner-Platz 1, 14109 Berlin, Germany

[a)]**Author to whom correspondence should be addressed:** anna.hassa@physik.uni-leipzig.de

ABSTRACT

A ternary, orthorhombic κ-$(Al_xGa_{1-x})_2O_3$ thin film was synthesized by combinatorial pulsed laser deposition on a 2 in. in diameter c-sapphire substrate with a composition gradient. Structural, morphological, and optical properties were studied as a function of the alloy composition. The thin film crystallized in the orthorhombic polymorph for Al contents of $0.07 \leq x \leq 0.46$, enabling bandgap engineering from 5.03 eV to 5.85 eV. The direct optical bandgap and the c-lattice constant, as well, show a linear dependence on the cation composition. XRD measurements, especially 2θ-ω- and ϕ-scans, revealed the growth of κ-$(Al_xGa_{1-x})_2O_3$ in [001]-direction and in three rotational domains. The surface morphology was investigated by atomic force microscopy and reveals root mean square surface roughnesses below 1 nm. Furthermore, the dielectric function (DF) and the refractive index, determined by spectroscopic ellipsometry, were investigated in dependence on the Al content. Certain features of the DF show a blue shift with increasing Al concentration.

I. INTRODUCTION

Monoclinic β-Ga_2O_3 can potentially be used in high-power electronics,[1–4] as solar-blind photo detectors,[5] gas sensors,[6] or thin film transistors,[7] because of its beneficial material properties such as a large Baliga's figure of merit, a large breakdown field[8] of 8 MV cm^{-1}, and a high bandgap energy of 4.6–5 eV.[3]

Another interesting polymorph of the wide bandgap material is its orthorhombic modification, denoted as κ-Ga_2O_3 and being isostructural to κ-Al_2O_3, making the growth of κ-$(Al,Ga)_2O_3$ for any cation composition seem possible. Ternary alloying enables the fabrication of thin films with tailored bandgaps[2–4] in a wide range, which leads to an extended application field. Up to now, just a few publications deal with the solubility limit of Al in κ-Ga_2O_3 or Ga in κ-Al_2O_3 as well as the dependence of chemical, structural, and optical properties on the cation composition. First investigations of orthorhombic $(Al_xGa_{1-x})_2O_3$ thin films grown on an AlN buffer layer on (00.1)Al_2O_3 for defined x were published by Tahara *et al.*[9] They report single phase thin films up to $x = 0.395$ with a direct optical bandgap of 5.9 eV. Storm *et al.* presented pulsed laser deposition (PLD) grown thin films on (00.1)Al_2O_3 with a maximum Al content of $x = 0.38$, which was increased by growth on a κ-Ga_2O_3 template up to $x = 0.65$.[10]

Binary κ-Ga_2O_3 can be fabricated by halide vapor phase epitaxy[11] (HVPE), atomic layer deposition[12] (ALD), metal-organic chemical vapor deposition[13–18] (MOCVD), plasma-assisted,[19] and tin-assisted[20] molecular beam epitaxy (MBE), as well as tin-assisted pulsed-laser deposition[21,22] (PLD). Alloys with In or Al were realized by mist CVD[9,23] and PLD[10,24,25] on c-plane sapphire substrates. The predicted large spontaneous polarization P of 23 $\mu C/cm^2$ along its c-axis[26] turns the orthorhombic structure, e.g., as κ-$(Al_xGa_{1-x})_2O_3$/κ-Ga_2O_3 heterostructure, to a promising alternative for the fabrication of high power devices. At the interface of heterostructures, P will change abruptly, resulting in an accumulation of free charge carriers.

In the present study, a κ-$(Al_xGa_{1-x})_2O_3$ thin film with a lateral variation of the alloy composition was grown by PLD using the continuous composition spread approach (CCS-PLD) described by von Wenckstern *et al.*[27] Tin was offered during growth to induce the orthorhombic phase as shown for binary κ-Ga_2O_3 by Kracht *et al.*[20] (MBE) and Kneiß *et al.*[22] (PLD). The highest achieved Al content in the present work amounts to $x = 0.46$. The chemical, structural, and optical material properties, namely crystal structure, surface morphology, optical bandgap energy, dielectric function, and refractive index will be discussed in dependence on the cation composition.

II. EXPERIMENTAL DETAILS

The ternary $(Al_xGa_{1-x})_2O_3$ thin film was grown by CCS-PLD using a two-fold segmented ceramic target. One segment consists of Ga_2O_3 (purity 99.999%, Alfa Aeser), and the other of Al_2O_3 (purity 99.997%, Alfa Aeser). Both have been admixed with 1.5 at. % SnO_2 to facilitate the growth in the orthorhombic structure. The oxygen partial pressure in the PLD chamber was 0.006 mbar and the growth temperature 640 °C. The KrF excimer laser radiation (248 nm) had an energy density of 2.6 J cm^{-2} on the target, which is located 10 cm away from the 2 in. in diameter (00.1)Al_2O_3 substrate. The pulse repetition frequency was 1 Hz for the first 300 pulses to create a nucleation layer and 10 Hz for the subsequent main layer, for which 30.000 pulses were applied. The chemical cation composition of the whole wafer was determined by energy-dispersive X-ray spectroscopy (EDX) performed with a FEI Nova Nanolab 200 equipped with an Ametek EDAX detector on 49 positions on the 2 in. wafer. Along the gradient, the cation concentration was additionally measured with higher spatial resolution by EDX as well as X-ray photoelectron spectroscopy (XPS). The XPS measurements were done at the Humboldt-Universität zu Berlin utilizing a JEOL JPS-9030 setup using non-monochromated Al K_α radiation for the excitation. The binding energy scale was referenced to C1s at 248.8 eV. The survey in Fig. 2 was recorded at the ENERGIZE endstation at Bessy II, using the Mg anode of a DAR400 X-ray source from ScientaOmicron for the excitation and a DA30 analyzer from ScientaOmicron for detection of the emitted photoelectrons. Here, the O1s peak was set to 531 eV, as the C1s peak was overlapped by Ga Auger peaks. Crystal structure screening was done with X-ray diffraction (XRD) measurements utilizing a PANalytical X'pert PRO MRD diffractometer equipped with a PIXcel^{3D} detector operating in 1D scanning line mode with 255 channels. The *c*-lattice constant for each detected XRD spectra was determined by fitting the (002), (004), (006), (008), and (0010) reflection peak positions with a pseudo-Voigt function, and subsequently, the lattice plane distances were extrapolated to a diffraction angle of $\theta = 90°$ using the formula $c = f(0.5[\tan(\theta)^{-1} + \cos(\theta)\tan(\theta)^{-1}])$ to minimize the goniometer error.[28] The direct optical bandgaps (E_g) were deduced from transmission measurements utilizing a PerkinElmer Lambda 19 spectrometer equipped with a deuterium lamp for the UV-region and a tungsten-halogen lamp for the visible and near-infrared region. From the transmission spectra (T), the absorption coefficient α was calculated via $\alpha = (-\ln(T)/d)^2$ with d being the film thickness. By extrapolation, the linear part of $(\alpha h\nu)^2$ to zero, E_g was estimated. Spectroscopic ellipsometry was employed to determine also E_g, d, the dielectric functions and refractive indexes utilizing a J.A. Woollam M2000 dual rotating compensator ellipsometer RC2 with a spot size of about $300 \times 500\ \mu m^2$.

III. RESULTS AND DISCUSSION

A. Structural properties

With the implemented CCS technique for thin film preparation, the cation concentration varies across the wafer. The resulting composition and the exact direction of the cation gradient was identified by EDX measurements on positions marked in Fig. 1(a) as black dots to determine the Al incorporation x, locally. In the figure, the compositions between the measurement points were interpolated, indicating the direction of the cation gradient. Additionally, along the gradient EDX and XPS mesurements were employed every mm (EDX) or every second mm (XPS). The Al content ranges from $x = 0.07$ to $x = 0.79$. These in principle identical results are presented in Fig. 1(b). In accordance with the surfactant-mediated growth model described by Kneiß *et al.*,[22] tin is not detected in the bulk (measured by EDX), but with the surface sensitive technique (XPS), tin-related peaks can be observed and are attributed to the Sn surfactant layer. The survey spectrum in Fig. 2 shows these tin peaks as well as peaks assigned to gallium, oxygen, and aluminum, as expected for $(Al_xGa_{1-x})_2O_3$.

The crystal structure was investigated in dependence on the Al content by 55 single XRD 2θ-ω scans recorded along the direction of the composition gradient. All measurements are presented as a false color map in Fig. 3(a). Three single XRD patterns for selected x values are depicted in Fig. 3(b). Over the whole composition range, reflection peaks of the c-sapphire substrate are visible at $2\theta = 41.58°$ and 90.64°. For $x > 0.46$, no additional reflections can be observed, which indicates the amorphous growth of $(Al_xGa_{1-x})_2O_3$ in this composition range. For $x \leq 0.46$, reflection peaks assigned to the (002) *n*-lattice planes of the orthorhombic crystal structure are visible.

The 2θ angles of these reflections shift with increasing Al content to higher values, due to the smaller ionic radius of Al compared to that of Ga. In accordance to this, the c-lattice constant, presented in Fig. 4(a), decreases with increasing x and shows two slightly different linear dependencies described by

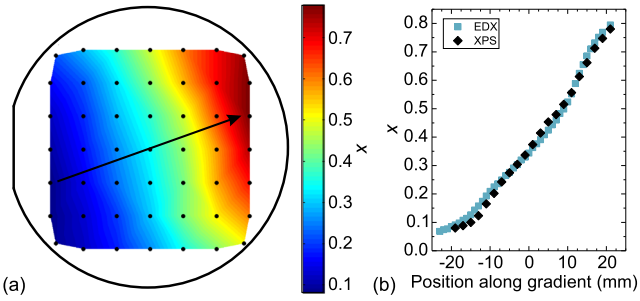

FIG. 1. (a) Al content x at 49 points across the thin film surface, marked in the graph as black dots and determined by EDX. The data between the measurement points was interpolated, the black arrow represents the direction of the gradient. (b) Cation ratio x acquired along the in (a) indicated gradient by EDX and XPS, respectively.

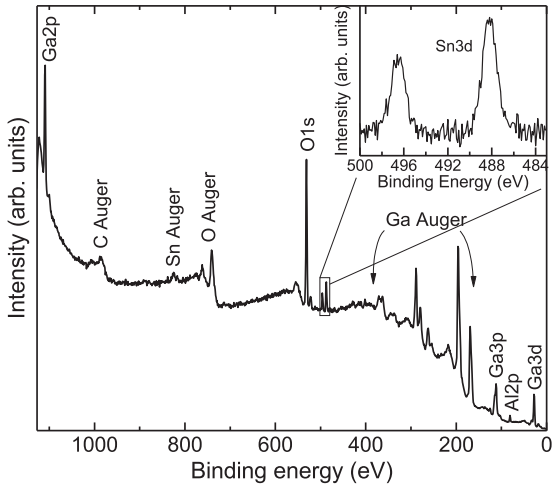

FIG. 2. XPS survey spectrum for $(Al_xGa_{1-x})_2O_3$.

$$c(x)(\text{Å}) = \begin{cases} (9.271 \pm 0.001) - (0.333 \pm 0.008) \cdot x, & \text{for } 0.07 \le x \le 0.13 \\ (9.276 \pm 0.001) - (0.357 \pm 0.002) \cdot x, & \text{for } 0.14 \le x \le 0.46. \end{cases} \quad (1)$$

For higher Al-contents ($x > 0.46$) the c-lattice constant saturates, indicating the solubility limit of κ-$(Al_xGa_{1-x})_2O_3$. Further, to investigate the crystalline quality of the thin film, the full width half maximum (FWHM) of the (004)-lattice plane reflection peaks is plotted in Fig. 4(a) in dependence on x exhibiting an increase from 0.07° for $x = 0.07$ to 0.15° for $x = 0.46$, indicating a high crystalline quality over the whole composition range. Comparisons with binary κ-Ga_2O_3 thin films grown by PLD on c-sapphire reveal similarly FWHM's of the (004) reflections below 0.06° for various growth temperatures and pressures.[22] XRD ϕ-scans of the skew-symmetric (131) and asymmetric (206) reflections, exemplarily shown in Fig. 4(b) for an Al concentration of $x = 0.13$, indicate the epitaxial growth on c-plane sapphire as well as the appearance of three rotational domains of the orthorhombic unit cell separated by 120°,[29] which were also present for κ-Ga_2O_3[22]

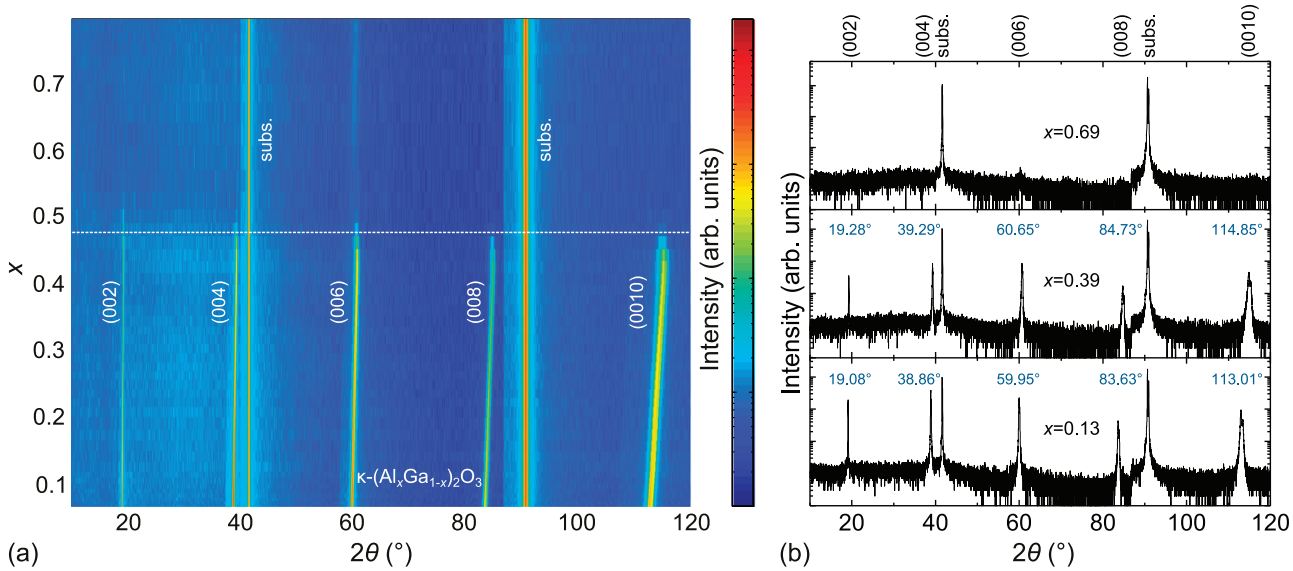

FIG. 3. (a) False color map of 2θ-ω scans of orthorhombic κ-$(Al_xGa_{1-x})_2O_3$ recorded along the composition gradient indicated in Fig. 1(a). (b) XRD patterns for $x = 0.13$, $x = 0.39$, and $x = 0.69$. Peak positions of the (002) n lattice planes as well as the substrate (subs.) reflection are labeled.

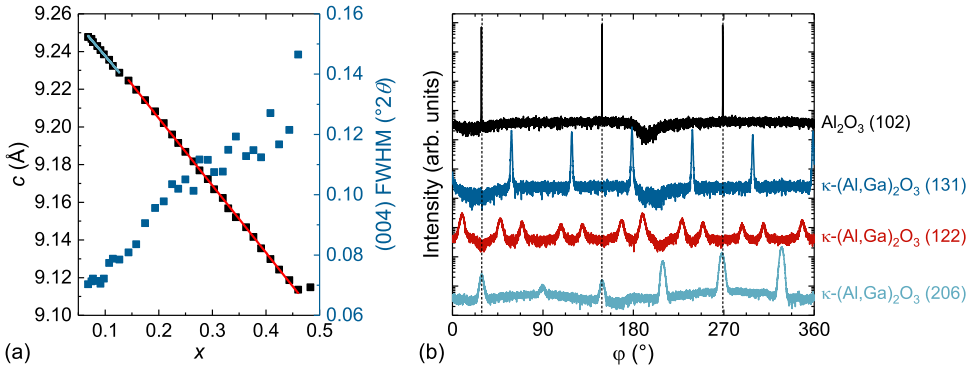

FIG. 4. (a) c lattice constant, estimated from the (002) n (n = 1–5) reflection peaks, as well as FWHM of the (004)-lattice plane reflection peak from XRD patterns determined in dependence on x. (b) XRD ϕ-scans of the (131), (122) and (206) reflections as well as the substrate (102) reflection performed for $x = 0.13$.

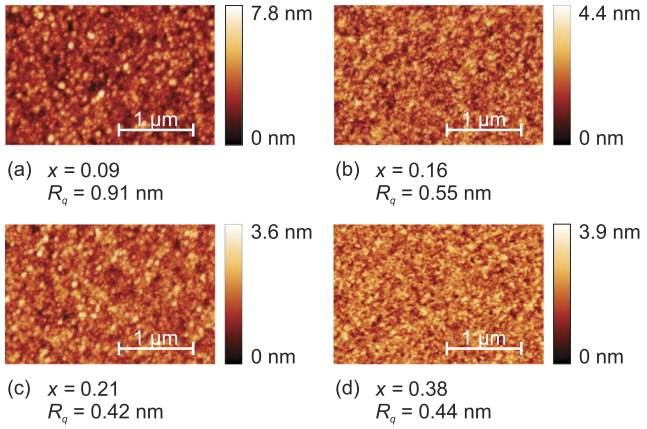

FIG. 5. 2 × 3 μm^2 AFM scans of surface morphologies of κ-$(Al_xGa_{1-x})_2O_3$ for different Al contents x as labeled recorded by AFM. R_q denotes the root mean square surface roughness.

and κ-$(In_xGa_{1-x})_2O_3$[24] thin films grown by PLD. The in-plane epitaxial relationships can be described by κ-$(Al_xGa_{1-x})_2O_3$ ⟨010⟩ ‖ α-Al_2O_3 ⟨10$\bar{1}$0⟩ and κ-$(Al_xGa_{1-x})_2O_3$ ⟨100⟩ ‖ α-Al_2O_3 ⟨2$\bar{1}\bar{1}$0⟩. Furthermore, the twelve-fold (122) reflection, originating from an additional two-fold splitting on mirror planes, proofs the orthorhombic structure of the thin film.

B. Surface morphology

The surface morphology was recorded along the cation gradient by atomic force microscopy. Exemplary images for four different Al-contents (x = 0.09, 0.16, 0.21, and 0.38) are shown in Fig. 5 and exhibit smooth surfaces consisting of spherically shaped grains with diameters of approximately 100 nm. Based on the recorded images, root mean square surface roughnesses (R_q) and corresponding peak-valley-distances (d_{PV}, described by the scale next to the recorded images) were determined. For $x \leq 0.21$, R_q and d_{PV} decrease with increasing x and stay roughly constant for $x > 0.21$.

C. Optical properties

The determination of the direct optical bandgap E_g in dependence on x was performed by two different measurement methods. Along the composition gradient, transmission spectroscopy and spectroscopic ellipsometry measurements were conducted. The first one was performed in 5 mm steps starting after 4 mm (equals 6 positions) and the second one in 1 mm steps (equals 32 positions) only on the κ-phase part of the thin film. Figure 6(a) presents transmission spectra as well as the calculated absorption spectra for different Al contents. The bandgap energies $E_{g,T}$ were obtained by extrapolating the linear part of the absorption spectra expressed as $(\alpha h\nu)^2$ to the zero line. The resulted direct optical bandgaps show a shift to higher energies with increasing x, which is also visible in Fig. 6(b). Linear fitting of $E_{g,T}$ yields

$$E_{g,T}(x)(\mathrm{eV}) = (4.92 \pm 0.06) + (2.17 \pm 0.08) \cdot x. \quad (2)$$

For comparison, the bandgap variation was determined via spectroscopic ellipsometry and is displayed in Fig. 6(b), too. The deduced change of the bandgap energy is almost linear and resulted in the fitting equation,

$$E_{g,E}(x)(\mathrm{eV}) = (4.85 \pm 0.01) + (2.14 \pm 0.03) \cdot x. \quad (3)$$

The resulting maximum bandgap energy is 5.85 eV for x = 0.46. In a previous publication of Schmidt-Grund *et al.*,[30] optical properties of an $(Al_xGa_{1-x})_2O_3$ thin film with the CCS-PLD technique on a 2 in. (001)-oriented MgO substrate was discussed. For $x < 0.4$, they observed the monoclinic β-modification and estimated the direct optical bandgap for this phase from spectroscopic ellipsometry to $E_{g-dir}(x)(\mathrm{eV}) = 4.811 + 2.138 \cdot x$. This is in accordance to the presented $E_{g,E}$ in our study, indicating a similar bandgap dependence of monoclinic and orthorhombic $(Al_xGa_{1-x})_2O_3$. The film thicknesses deduced from the spectroscopic ellipsometry data were divided by the applied pulse number to obtain the composition dependent growth rate $r(x)$ that is displayed in Fig. 6(b), too. It exhibits a maximum of 15.7 pm/pulse for x = 0.07 and decreases to 12.0 pm/pulse for x = 0.46.

Further, the dielectric function (DF) was obtained by using a layer stack model consisting of a c-plane sapphire substrate layer, where the DF was taken from literature,[31] a layer describing the thin film and a surface layer. Due to the presence of rotational domains, the film is effectively optical uniaxial, i.e., the tensor of the film DF is given by $\varepsilon_\perp = \varepsilon_{xx} = \varepsilon_{yy} \neq \varepsilon_\parallel = \varepsilon_{zz}$ and $\varepsilon_{ij} = 0$ for $i \neq j$. The line shape of each tensor component was described by model dielectric functions. Due to the absence of sharp features in the experimental spectra, it was sufficient to describe the onset of the absorption in

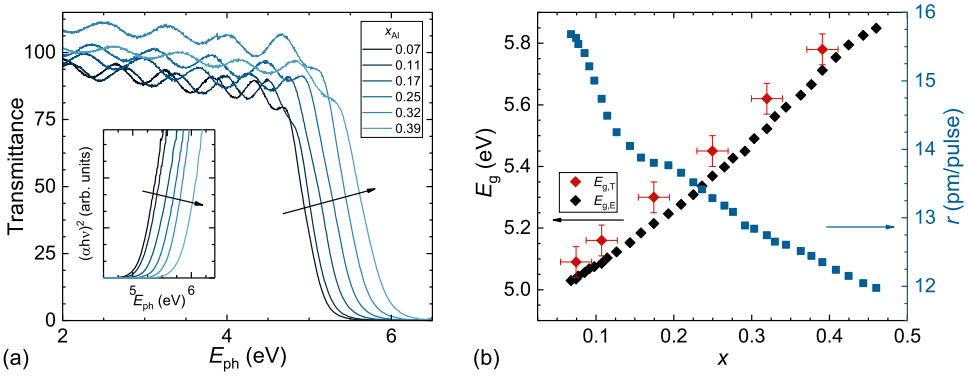

FIG. 6. (a) Transmission spectra for increasing Al contents as labeled. The inset shows corresponding absorption spectra expressed as $(\alpha h\nu)^2$. (b) Direct optical bandgap and growth rate r as a function of x. The values are determined by transmission spectroscopy [$E_{g,T}$, shown in (a)] by and spectroscopic ellipsometry ($E_{g,E}$), respectively.

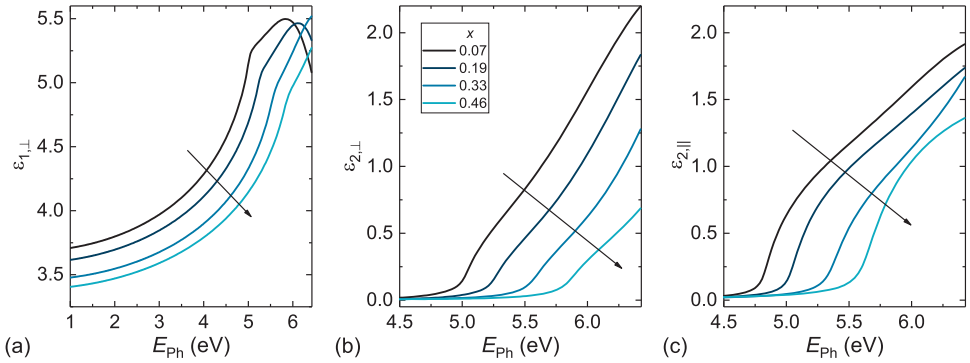

FIG. 7. Real (a) and imaginary part [(b) and (c)] of the dielectric function for different Al concentration as labeled.

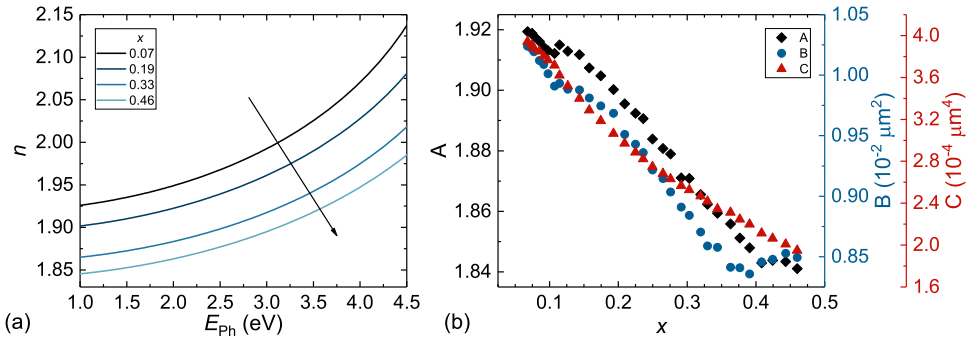

FIG. 8. (a) Refractive index n depending on the photon energy for various x as labeled. (b) Cauchy parameters A, B, and C in dependence of x.

the observed spectral range by band-to-band transitions ($\chi^{\mathrm{CPM_0}}$) as proposed by Adachi.[32] The contributions of the energetic transitions to the imaginary part of the DF is described by Gaussian oscillators (χ^{gauss}), whereas the contributions of these transitions to the real part of the DF was described by means of a pole function (χ^{pole}) due to the Kramers-Kronig transformation. Thus, the entire DF for each component is given by

$$\varepsilon_i = 1 + \sum_{j=1}^{2} \chi_{j,i}^{\mathrm{CPM_0}} + \chi_{j,i}^{\mathrm{gauss}} + \chi_i^{\mathrm{pole}}, \tag{4}$$

with $i = \perp, \parallel$. Finally, the dielectric function of the surface layer was described by an effective medium approach,[33] where the dielectric function of the underlaying $(Al,Ga)_2O_3$ film and void was mixed 1:1.

The DF for various x is presented in Fig. 7 and shows that incorporation of Al leads to a blue shift of the transition energies and thus to a blue shift of the entire dielectric function. This is accompanied by a decrease of the real part of the DF in the visible spectral range and thus of the refractive index displayed in Fig. 8(a). A comparison of the tensor components yields that the absorption sets in at lower energies for light polarized parallel to the surface normal than for light polarized perpendicular to the surface normal. Additionally, the Cauchy function $n = A + B/\lambda^2 + C/\lambda^4$ describes the dispersion of the refractive index up to 4.5 eV. Figure 8(b) presents the Cauchy parameters A, B, and C as a function of x.

IV. CONCLUSION

In this study, an orthorhombic $(Al_xGa_{1-x})_2O_3$ thin film with a lateral varying cation composition gradient ($0.07 \leq x \leq 0.46$) was examined for a variety of structural and optical material properties in dependence on x. For the highest Al incorporation of $x = 0.46$ in the crystalline phase, the optical bandgap at RT is 5.85 eV, which is up to now the highest reported Al content and E_G for κ-$(Al_xGa_{1-x})_2O_3$ thin films grown on c-plane sapphire. Chemical investigations confirmed a tin enrichment on the layer surface, not in the bulk, indicating a surfactant-mediated growth of the thin film. Heteroepitaxial growth in three rotational domains was presented and compared to heteroepitaxial grown monoclinic thin films, the sample shown here has higher crystalline quality, higher growth rates, and lower surface roughnesses. The c-lattice constant exhibits a linear increase with increasing x following Vegard's law. Furthermore, dielectric functions and refractive indexes were investigated in a wide composition range. Based on our findings, κ-$(Al_xGa_{1-x})_2O_3$ seems to be well suited for possible usage, e.g., in high electron mobility transistors, as wave-length selective UV - or quantum-well infrared photodetectors and more. Future investigations should target the suppression of rotational domains as well as doping to achieve electrically conductive samples.

ACKNOWLEDGMENTS

We thank Monika Hahn for PLD target fabrication, Jörg Lenzner for EDX measurements, and Ulrike Teschner for transmission measurements. This work was supported by the European Social Fund within the Young Investigator Group "Oxide Heterostructures" (Grant No. SAB 100310460) and partly by Deutsche Forschungsgemeinschaft in the Framework of Sonderforschungsbereich 762 "Functionality of Oxide Interfaces". A.H. and M.K. acknowledge the Leipzig School for Natural Sciences BuildMoNa.

We acknowledge support from the German Research Foundation (DFG) and Universität Leipzig within the program of Open Access Publishing. The work in Berlin was funded by the Deutsche Forschungsgemeinschaft (DFG) - Projekt No. 182087777-SFB 951.

REFERENCES

[1]M. Higashiwaki, A. Kuramata, H. Murakami, and Y. Kumagai, "State-of-the-art technologies of gallium oxide power devices," J. Phys. D: Appl. Phys. **50**, 333002 (2017).
[2]S. Stepanov, V. Nikolaev, V. Bougrov, and A. Romanov, "Gallium oxide: Properties and applications—A review," Rev. Adv. Mater. Sci. **44**, 63–86 (2016).
[3]H. von Wenckstern, "Group-III sesquioxides: Growth, physical properties and devices," Adv. Electron. Mater. **3**, 1600350 (2017).
[4]S. J. Pearton, J. Yang, P. H. Cary, F. Ren, J. Kim, M. J. Tadjer, and M. A. Mastro, "A review of Ga_2O_3 materials, processing, and devices," Appl. Phys. Rev. **5**, 011301 (2018).
[5]Z. Zhang, H. von Wenckstern, and M. Grundmann, "Monolithic multichannel ultraviolet photodiodes based on (Mg,Zn)O thin films with continuous composition spreads," IEEE J. Sel. Top. Quantum Electron. **20**, 106–111 (2014).
[6]O. Bierwagen, "Indium oxide—A transparent, wide-band gap semiconductor for (opto)electronic applications," Semicond. Sci. Technol. **30**, 024001 (2015).
[7]M. Grundmann, H. Frenzel, A. Lajn, M. Lorenz, F. Schein, and H. von Wenckstern, "Transparent semiconducting oxides: Materials and devices," Phys. Status Solidi A **207**, 1437–1449 (2010).
[8]M. Higashiwaki, K. Sasaki, A. Kuramata, T. Masui, and S. Yamakoshi, "Gallium oxide (Ga_2O_3) metal-semiconductor field-effect transistors on single-crystal β-Ga_2O_3 (010) substrates," Appl. Phys. Lett. **100**, 013504 (2012).
[9]D. Tahara, H. Nishinaka, S. Morimoto, and M. Yoshimoto, "Heteroepitaxial growth of ε-$(Al_xGa_{1-x})_2O_3$ alloy films on c-plane AlN templates by mist chemical vapor deposition," Appl. Phys. Lett. **112**, 152102 (2018).
[10]P. Storm, M. Kneiß, A. Hassa, T. Schultz, D. Splith, H. von Wenckstern, N. Koch, M. Lorenz, and M. Grundmann, "Epitaxial κ-$(Al_xGa_{1-x})_2O_3$ thin films and heterostructures grown by tin-assisted VCCS-PLD," APL Mater. **7**, 111110 (2019).
[11]Y. Oshima, E. G. Víllora, Y. Matsushita, S. Yamamoto, and K. Shimamura, "Epitaxial growth of phase-pure ε-Ga_2O_3 by halide vapor phase epitaxy," J. Appl. Phys. **118**, 085301 (2015).
[12]F. Boschi, M. Bosi, T. Berzina, E. Buffagni, C. Ferrari, and R. Fornari, "Hetero-epitaxy of ε-Ga_2O_3 layers by MOCVD and ALD," J. Cryst. Growth **443**, 25–30 (2016).
[13]I. Cora, F. Mezzadri, F. Boschi, M. Bosi, M. Čaplovičová, G. Calestani, I. Dódony, B. Pécz, and R. Fornari, "The real structure of ε-Ga_2O_3 and its relation to κ-phase," CrystEngComm **19**, 1509–1516 (2017).
[14]X. Xia, Y. Chen, Q. Feng, H. Liang, P. Tao, M. Xu, and G. Du, "Hexagonal phase-pure wide band gap ε-Ga_2O_3 films grown on 6H-SiC substrates by metal organic chemical vapor deposition," Appl. Phys. Lett. **108**, 202103 (2016).
[15]F. Mezzadri, G. Calestani, F. Boschi, D. Delmonte, M. Bosi, and R. Fornari, "Crystal structure and ferroelectric properties of ε-Ga_2O_3 films grown on (0001)-sapphire," Inorg. Chem. **55**, 12079–12084 (2016).
[16]Y. Chen, X. Xia, H. Liang, Q. Abbas, Y. Liu, and G. Du, "Growth pressure controlled nucleation epitaxy of pure phase ε- and β-Ga_2O_3 films on Al_2O_3 via MOCVD," Cryst. Growth Des. **18**, 1147–1154 (2018).
[17]M. Pavesi, F. Fabbri, F. Boschi, G. Piacentini, A. Baraldi, M. Bosi, E. Gombia, A. Parisini, and R. Fornari, "ε-Ga_2O_3 epilayers as a material for solar-blind UV photodetectors," Mater. Chem. Phys. **205**, 502–507 (2018).
[18]M. Mulazzi, F. Reichmann, A. Becker, W. M. Klesse, P. Alippi, V. Fiorentini, A. Parisini, M. Bosi, and R. Fornari, "The electronic structure of ε-Ga_2O_3," APL Mater. **7**, 022522 (2019).
[19]P. Vogt, O. Brandt, H. Riechert, J. Lähnemann, and O. Bierwagen, "Metal-exchange catalysis in the growth of sesquioxides: Towards heterostructures of transparent oxide semiconductors," Phys. Rev. Lett. **119**, 196001 (2017).
[20]M. Kracht, A. Karg, J. Schörmann, M. Weinhold, D. Zink, F. Michel, M. Rohnke, M. Schowalter, B. Gerken, A. Rosenauer, P. J. Klar, J. Janek, and M. Eickhoff, "Tin-assisted synthesis of ε−Ga_2O_3 by molecular beam epitaxy," Phys. Rev. Appl. **8**, 054002 (2017).
[21]M. Orita, H. Hiramatsu, H. Ohta, M. Hirano, and H. Hosono, "Preparation of highly conductive, deep ultraviolet transparent β-Ga_2O_3 thin film at low deposition temperatures," Thin Solid Films **411**, 134–139 (2002).
[22]M. Kneiß, A. Hassa, D. Splith, C. Sturm, H. von Wenckstern, T. Schultz, N. Koch, M. Lorenz, and M. Grundmann, "Tin-assisted heteroepitaxial PLD-growth of κ-Ga_2O_3 thin films with high crystalline quality," APL Mater. **7**, 022516 (2019).
[23]H. Nishinaka, N. Miyauchi, D. Tahara, S. Morimoto, and M. Yoshimoto, "Incorporation of indium into ε-gallium oxide epitaxial thin films grown via mist chemical vapour deposition for bandgap engineering," CrystEngComm **20**, 1882–1888 (2018).
[24]A. Hassa, H. von Wenckstern, D. Splith, C. Sturm, M. Kneiß, V. Prozheeva, and M. Grundmann, "Structural, optical, and electrical properties of orthorhombic κ-$(In_xGa_{1-x})_2O_3$ thin films," APL Mater. **7**, 022525 (2019).
[25]M. Kneiß, A. Hassa, D. Splith, C. Sturm, H. von Wenckstern, M. Lorenz, and M. Grundmann, "Epitaxial stabilization of single phase κ-$(In_xGa_{1-x})_2O_3$ thin films up to $x = 0.28$ on c-sapphire and κ-Ga_2O_3 (001) templates by tin-assisted VCCS-PLD," APL Mater. **7**, 101102 (2019).
[26]M. B. Maccioni and V. Fiorentini, "Phase diagram and polarization of stable phases of $(Ga_{1-x}In_x)_2O_3$," Appl. Phys. Express **9**, 041102 (2016).
[27]H. von Wenckstern, Z. Zhang, F. Schmidt, J. Lenzner, H. Hochmuth, and M. Grundmann, "Continuous composition spread using pulsed-laser deposition with a single segmented target," CrystEngComm **15**, 10020 (2013).
[28]L. Spiess, G. Teichert, R. Schwarzer, H. Behnken, and C. Genzel, *Moderne Röntgenbeugung: Röntgendiffraktometrie für Materialwissenschaftler, Physiker und Chemiker*, German ed. (Vieweg+Teubner Verlag, 2009).
[29]M. Grundmann, "Formation of epitaxial domains: Unified theory and survey of experimental results," Phys. Status Solidi B **248**, 805–824 (2011).
[30]R. Schmidt-Grund, C. Kranert, H. von Wenckstern, V. Zviagin, M. Lorenz, and M. Grundmann, "Dielectric function in the spectral range (0.5–8.5)eV of an $(Al_xGa_{1-x})_2O_3$ thin film with continuous composition spread," J. Appl. Phys. **117**, 165307 (2015).
[31]H. Yao and C. H. Yan, "Anisotropic optical responses of sapphire (α-Al_2O_3) single crystals," J. Appl. Phys. **85**, 6717 (1999).
[32]S. Adachi, "Model dielectric constants of GaP, GaAs, GaSb, InP, InAs, and InSb," Phys. Rev. B **35**, 7454–7463 (1987).
[33]D. A. G. Bruggeman, Ann. Phys. **24**, 636 (1935).